Geodesic of nonlinear electrodynamics and stable photon orbits

A. S. Habibina[*] and H. S. Ramadhan[†]

Departemen Fisika, FMIPA, Universitas Indonesia, Depok 16424, Indonesia

(Received 3 February 2020; revised manuscript received 11 May 2020; accepted 19 May 2020; published 18 June 2020)

We study the geodesics of charged black holes in polynomial Maxwell Lagrangians, a subclass of models within the nonlinear electrodynamics (NLED). Specifically, we consider black holes in Kruglov, power-law, and Ayon-Beato-Garcia models. Our exploration on the corresponding null bound states reveals that a photon can orbit the extremal black holes in stable radii outside the corresponding horizon, contrary to the case of the Reissner-Nordstrom black holes. The reason behind this is the well-known theorem that a photon in a NLED background propagates along its own *effective* geometry. This nonlinearity is able to shift the local minimum of the effective potential away from its corresponding outer horizon. For the null scattering states, we obtain corrections to the weak deflection angle off the black holes. We rule out the power-law model to be physical since its deflection angle does not reduce to the Schwarzschild in the limit of the vanishing charge.

DOI: 10.1103/PhysRevD.101.124036

I. INTRODUCTION

One of the many intriguing properties of a black hole (BH) is the notion of the *photon sphere*, the path upon which null rays can orbit in a constant radius. The recent profound observation of a black hole is made possible by producing the ringlike image of a photon sphere around the supermassive BH [1]. This discovery relies on the rather realistic rotating BH, whose (circular as well as spherical) photon orbits have extensively been investigated, for example, in [2,3] and the references therein. It is nevertheless also of high interest to study the photon sphere in static cases. The Schwarzschild BH is known to have an (unstable) null orbit at $r = 3M$ in natural unit. The Reissner-Nordstrom (RN) black hole possesses two photon spheres $r_{ps}^{\pm} = \frac{3M}{2}\left(1 \pm \sqrt{1 - \frac{8}{9}(\frac{Q}{M})^2}\right)$, only one of which (r_+) can be observed since it lies outside its outer horizon. This physical orbit is the local maximum of the corresponding effective null potential; thus, it is also unstable. As pointed out in [4,5], the extremal RN black hole can have a stable photon orbit exactly *on* its (extreme) horizon, r_{EH}.

Nonlinear electrodynamics (NLED) is not new in modern physics. Mie in 1912 and later, Born and Infeld in 1934 proposed that an electron is a nonsingular solution of field theory with a finite electromagnetic energy [6,7]. With the development of quantum electrodynamics (QED), these classical nonlinear field theories were later abandoned. Ironically, it is precisely the success of QED that resurrects the recent interest in NLED. Recent photon-photon scattering experimental results strongly indicate that in the vacuum, electrodynamics might be nonlinear [8–11]. Euler and Heisenberg predicted that vacuum magnetic birefringence must occur in QED [12]. This phenomenon is absent in Maxwell and Born-Infeld (BI) electrodynamics but can be present in other NLED. The bound for the birefringence's magnitude is provided by the BMV and PVLAS experiments [13–15], and improvements are still being sought. It is then no wonder that in the recent decade, there are abundant proposals for NLED. Kruglov proposed a generalization of BI electrodynamics as a model for fractional electrodynamics [16,17] and a few nonlinear electrodynamics models with trigonometric terms [18,19]. Euler-Heisenberg electrodynamics, which features second order Maxwell electrodynamics, was revisited in [20,21]. Logarithmic electrodynamics was investigated in [22,23], while exponential electrodynamics along with its phenomenology were studied in [24–26]. The first black hole solutions coupled with a nonlinear charge was discussed by Hoffmann and Infeld and by Peres [27,28]. They presented exact solutions of the Einstein-Born-Infeld (EBI) theory. Today, several exact solutions of black holes charged with NLED sources, both in general relativity (GR) as well as in modified gravity, have extensively been explored (see, for example, [29–38] and references therein). The cosmological effect of a form of NLED with one parameter was examined in [39,40]. Some of the most studied models of NLED are the conformally invariant power Maxwell electrodynamics, which were analyzed as higher-dimensional black holes in [41,42], and the Ayon-Beato-Garcia electrodynamics, which were developed using a Hamiltonian formulation to construct an

[*]a.sayyidina@sci.ui.ac.id
[†]hramad@sci.ui.ac.id

 © 2020 American Physical Society

electrically charged Bardeen's regular black hole solution in [43], and the magnetically charged one on [44], where it was resurfaced in recent studies [45,46].

It is well-known that a photon behaves differently in the NLED ambient compared to the linear Maxwell electrodynamics. They do not propagate along the background geometry's null geodesic. Rather, they follow the null geodesic of its effective geometry [47]. This behavior sheds light on the photon sphere study on charged BH. Curiously, research on this topic is rather rare.[1] It is therefore of our interest to study this phenomenology in the vast literature of NLED models. In this work, we shall investigate the null geodesic of several NLED models in the framework of GR. For simplicity, in this preliminary work, we shall focus on the polynomial Maxwell-type Lagrangians. That is, we consider three models: the Kruglov, the power-law Maxwell, and the Ayon-Beato-Garcia NLED models.

This work is organized as follows. In Sec. II, we give a brief overview of the general NLED model. Sections III–V are devoted to investigating the three different NLED models. In each, we study their timelike and null geodesics, as well as the weak deflection angle of light. We completely reproduce the photon orbit values for each model. Our conclusion is summarized in Sec. VI.

II. OVERVIEW OF NLED

In general, all NLED models can be expressed as a functional of Maxwell's Lagrangian, $\mathcal{L}=\mathcal{L}[\mathcal{F}]$, where[2] $\mathcal{F}\equiv\frac{1}{4}F_{\mu\nu}F^{\mu\nu}$. By the correspondence principle, in the low-energy/weak-coupling limit, they all should reduce to Maxwell, $\mathcal{L}=-\mathcal{F}$.

Any nonlinearization extension of an established theory must obey causality and unitary principles. In the context of electrodynamics, they can be formulated as the following constraints [50,51]:

$$\mathcal{L}_{\mathcal{F}}\leq 0, \qquad \mathcal{L}_{\mathcal{FF}}\geq 0, \qquad \mathcal{L}_{\mathcal{F}}+2\mathcal{F}\mathcal{L}_{\mathcal{FF}}\leq 0, \tag{1}$$

where $\mathcal{L}_{\mathcal{F}}\equiv\partial\mathcal{L}/\partial\mathcal{F}$ and $\mathcal{L}_{\mathcal{FF}}\equiv\partial^2\mathcal{L}/\partial\mathcal{F}^2$.

The field equation is given by its corresponding Euler-Lagrange,

$$\nabla_\mu(\mathcal{L}_{\mathcal{F}}F^{\mu\nu})=0. \tag{2}$$

Alternatively, one can define, by means of a Legendre transformation, the corresponding "Hamiltonian" [43,52],

$$\mathcal{H}\equiv 2\mathcal{L}_{\mathcal{F}}\mathcal{F}-\mathcal{L}. \tag{3}$$

The Lagrangian, in turn, can be written as

$$\mathcal{L}=2\mathcal{H}_{\mathcal{P}}\mathcal{P}-\mathcal{H}, \tag{4}$$

where $\mathcal{P}\equiv\frac{1}{4}P_{\mu\nu}P^{\mu\nu}$ and $P^{\mu\nu}\equiv\mathcal{L}_{\mathcal{F}}F^{\mu\nu}$. It is easy to see that $\mathcal{H}=\mathcal{H}[\mathcal{P}]$. The field equation is then given by

$$\nabla_\mu P^{\mu\nu}=0. \tag{5}$$

In any case, the field equations can be shown to be

$$\nabla\cdot\mathbf{D}=0, \qquad \frac{\partial\mathbf{D}}{\partial t}=\nabla\times\mathbf{H}, \tag{6}$$

with $\mathbf{D}\equiv\partial\mathcal{L}/\partial\mathbf{E}$ the electric displacement field and $\mathbf{H}\equiv-\partial\mathcal{L}/\partial\mathbf{B}$ the magnetic field. The nonlinearity implies the relation between $\mathbf{E}$ and $\mathbf{D}$ as well as $\mathbf{B}$ and $\mathbf{H}$ are not linear. In general, $\mathbf{D}=\mathbf{D}(\mathbf{E},\mathbf{B})$ and $\mathbf{H}=\mathbf{H}(\mathbf{E},\mathbf{B})$. One interesting phenomenological interpretation is that NLED describe the electromagnetic wave propagation in nonlinear media.

III. GENERALIZED BORN-INFELD

This model was proposed by Kruglov to generalize the BI electrodynamics [17],

$$\mathcal{L}_K=\frac{1}{\beta}\left[1-\left(1+\frac{\beta F}{q}\right)^q\right]. \tag{7}$$

Here, β is a parameter with a dimension of $[L]^4$, and q is an arbitrary dimensionless parameter. For $q=1$, the model reduces to Maxwell, while $q=1/2$ gives us BI electrodynamics. In flat spacetime, the field equation (2) yields

$$\partial_\mu(\Gamma^{q-1}F^{\mu\nu})=0, \qquad \Gamma\equiv 1+\frac{\beta\mathcal{F}}{q}. \tag{8}$$

This equation is equivalent to Eq. (6) with the following identifications:

$$\mathbf{D}=\varepsilon\mathbf{E}, \qquad \mathbf{H}=\mu^{-1}\mathbf{B}, \tag{9}$$

where $\varepsilon=\mu^{-1}\equiv\Gamma^{q-1}$. For an electric point-charge source, the displacement field $\mathbf{D}(r)$ is singular at the origin, but the electric field $\mathbf{E}(r)$ is not. It is regular at the core with a finite value given by $\mathbf{E}(0)=\sqrt{\frac{2q}{\beta}}$.

The monopole black hole can be obtained from the Einstein-Kruglov model [35],

$$S=\int d^4x\sqrt{-g}\left[\frac{R}{2\kappa^2}+\mathcal{L}_K\right], \tag{10}$$

where $\kappa^2\equiv 8\pi G$. The ansatz employed here is a magnetic monopole and has spherical symmetry [32],

$$A_t=A_r=A_\theta=0, \qquad A_\phi=Q(1-\cos\theta), \tag{11}$$

and

[1]The relations between photon spheres in Einstein-BI gravity with its phase transitions are studied in [48,49] and the references therein.

[2]Throughout this work, we shall not deal with $\mathcal{G}\equiv\frac{1}{4}F_{\mu\nu}\tilde{F}^{\mu\nu}$. This can be done by setting its constant parameter to be zero.

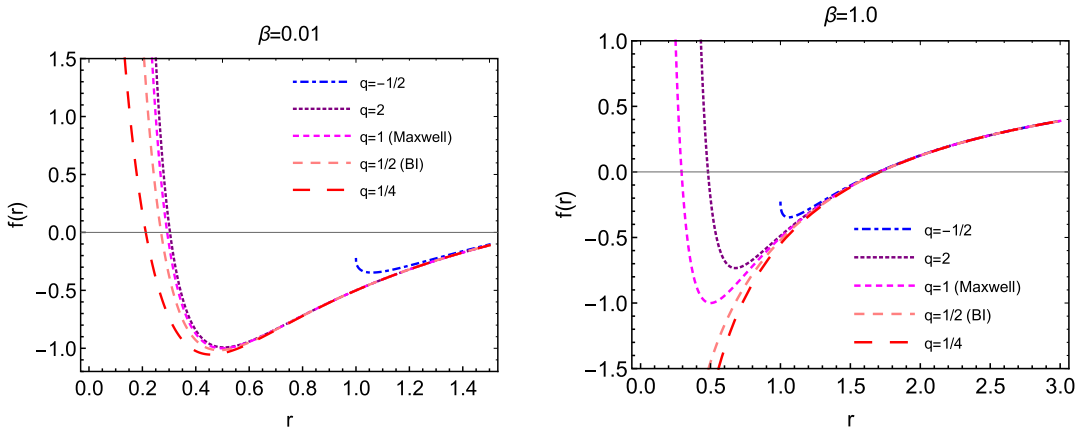

FIG. 1. Typical plots of $f(r)$ with $M = Q = 1$.

$$ds^2 = -f(r)dt^2 + f^{-1}(r)dr^2 + r^2 d\Omega^2. \tag{12}$$

The solutions are [35]

$$F_{\theta\phi} = Q\sin\theta, \tag{13}$$

and

$$f(r) = 1 - \frac{2M}{r} - \frac{\kappa^2 r^2}{3\beta}\left[{}_2F_1\left(-\frac{3}{4}, -q; \frac{1}{4}; -\frac{Q^2\beta}{2qr^4}\right) - 1\right], \tag{14}$$

where Q is the magnetic charge and ${}_2F_1(a, b; c; d)$ the hypergeometric function. It can be shown that in the limit of $\beta \to 0$, the solution reduces to the magnetic RN, while for $q \to 1/2$, it reduces to the magnetic BI black holes [29,34].

In Fig. 1, we show typical plots of the metric function for several values of q, both in the strong and the weak coupling regimes. The behavior does not differ much from the RN solution; they all typically have two horizons. For values of q that do not reduce to the Maxwell (for example, $q = -1/2$), the metric stops being real. Since they generally possess two horizons, in principle, the metric (14) can be extremal. While it is impossible to show the extremal condition for M and Q analytically, in Fig. 2, we show that the extremal conditions can be satisfied for certain values of the parameters. The radius tangent to the minima of the metric is the extremal horizon $r_{\rm EH}$. As β goes stronger, $r_{\rm EH}$ shifts *closer* to the singularity. However, for $q < 1$, there is a critical value of β above which only one horizon exists. This can be seen in Fig. 1 on the right. For completion, in Fig. 3 we show the case for naked singularity.

A. Timelike geodesics

A test particle with a mass μ and (electric/magnetic) charge ϵ around a compact object can be described by the geodesics equation [34],

$$\frac{d^2x^\nu}{d\tau^2} + \Gamma^\nu_{\alpha\beta}\frac{dx^\alpha}{d\tau}\frac{dx^\beta}{d\tau} = -\frac{\epsilon}{\mu}F^\nu_\sigma\frac{dx^\sigma}{d\tau}. \tag{15}$$

For our metric (12), the timelike geodesics on an equatorial plane ($\theta = \pi/2$) can be written as

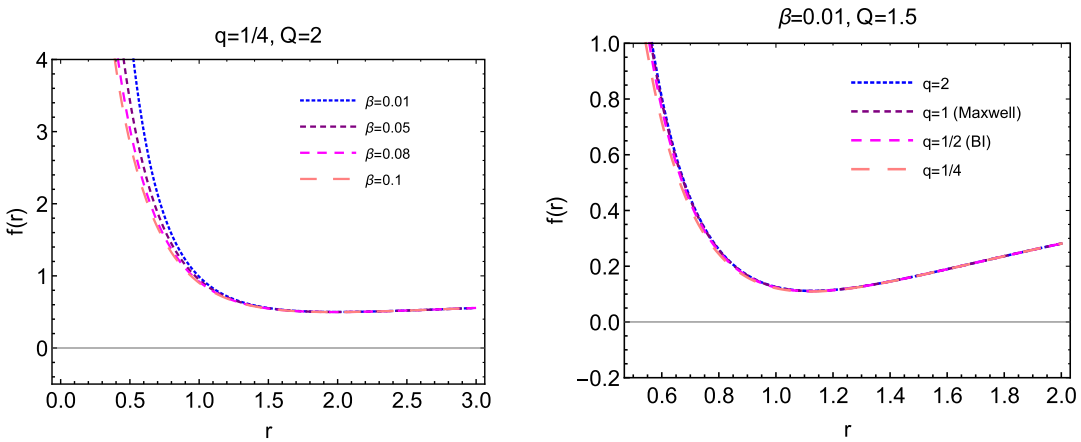

FIG. 2. The cases naked singularities of the metric function $f(r)$. [Left] The no-horizon solution with fixed q for several values of β [Right] and vice versa. Here, we set $M = 1$.

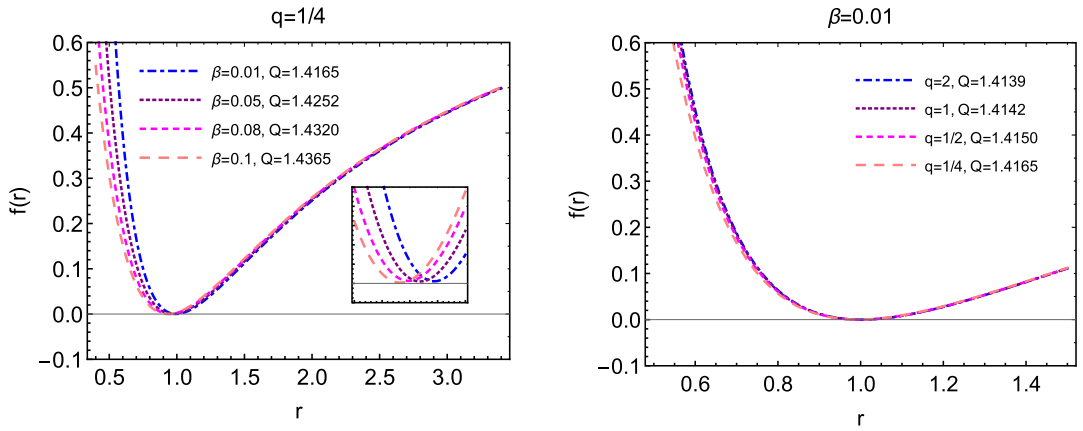

FIG. 3. Typical of extremal cases of the metric function $f(r)$. [Left] The extremal solution with fixed q for several values of β [Right] and vice versa. Here, we set $M = 1$.

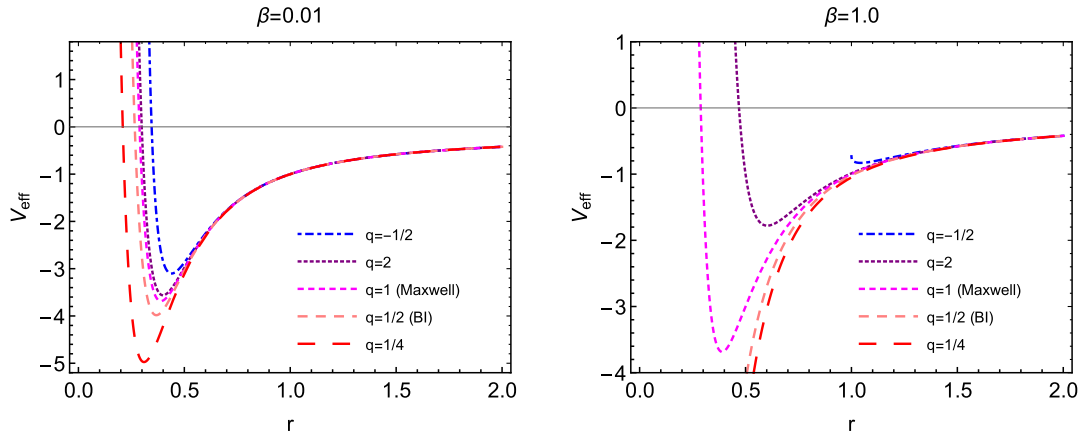

FIG. 4. The effective potential for massive particles Eq. (19) with $M = Q = 1$.

$$1 = f\dot{t}^2 - f^{-1}\dot{r}^2 - r^2\dot{\phi}^2. \tag{16}$$

The symmetry of the metric admits conserved quantities,

$$\dot{t} = \frac{\mathbb{E}}{f}, \qquad \dot{\phi} = \frac{\mathbb{L}}{r^2}, \tag{17}$$

where $\mathbb{E}$ and $\mathbb{L}$ are the energy-and angular momentum-per unit mass of the test charged particles, respectively. Equation (16) can be rewritten as

$$\dot{r}^2 + f\left(\frac{\mathbb{L}^2}{r^2} + 1\right) - \mathbb{E}^2 = 0. \tag{18}$$

Comparing the equation to $\frac{1}{2}\dot{r} + V_{\rm eff}(r) = 0$, we can extract the effective potential as

$$V_{\rm eff}(r) = \frac{1}{2}\left(\frac{\mathbb{L}^2}{r^2}+1\right)\left(1-\frac{2M}{r}-\frac{\kappa^2 r^2}{3\beta} \times \left[{}_2F_1\left(-\frac{3}{4},-q;\frac{1}{4};-\frac{Q^2\beta}{2qr^4}\right)-1\right]\right)-\frac{\mathbb{E}^2}{2}. \tag{19}$$

It is interesting to note that for a monopole black hole, a massive charged (either electrically or magnetically) test particle behaves the same as the chargeless one.

The plot of $V_{\rm eff}(r)$ for several values of q are shown in Fig. 4. Here, we set $\mathbb{E} = \mathbb{L} = 1$. The feature of $V_{\rm eff}(r)$ is qualitatively the same as the Newtonian counterpart; there exists bounded orbits. The minimum of $V_{\rm eff}(r)$ corresponds to the radius of a *stable circular orbit*[3] $r_{\rm SCO}$, while its local maximum represents the radius of an unstable circular orbit $r_{\rm UCO}$. These closed orbits are constrained by q and the

[3]To be precise, here, $r_{\rm SCO} = r_{\rm SCO}(M, Q, q, \beta)$. The smallest $r_{\rm SCO}$ that corresponds to the minimum of hypersurface $r_{\rm SCO}$ is the (M, Q, q, β) hyperspace and is called *the innermost stable circular orbit*, $r_{\rm ISCO}$.

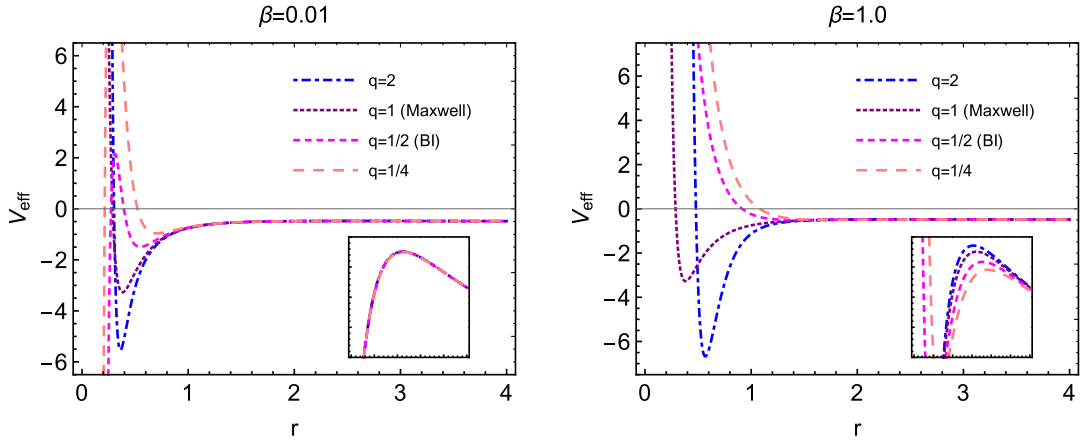

FIG. 5. The effective potential for massless particles (25) in the nonextremal case. Here, we set $M = Q = 1$.

nonlinear coupling β. For $q \leq -1/2$, the $V_{\rm eff}(r)$ stops being real.

B. Null geodesics

Novello *et al.* showed that in NLED, a photon follows the null geodesic of its *effective* geometry given by [47]

$$g^{\mu\nu}_{\rm eff} = \mathcal{L}_{\mathcal{F}} g^{\mu\nu} - 4\mathcal{L}_{\mathcal{F}\mathcal{F}} F^{\mu}{}_{\alpha} F^{\alpha\nu}. \tag{20}$$

For our case, it is given by

$$g^{\mu\nu}_{\rm eff} = \left(1 + \frac{\beta F}{q}\right) g^{\mu\nu} - \frac{4\beta(q-1)}{q} F^{\mu\alpha} F^{\nu}_{\alpha}. \tag{21}$$

Defining a factor $h(r) \equiv \frac{2qr^4+\beta Q^2}{\beta(8q-7)Q^2+2qr^4}$, the *conformally rescaled* effective line element can be written as

$$ds^2_{\rm eff} = -f(r)dt^2 + f(r)^{-1}dr^2 + h(r)r^2 d\Omega^2. \tag{22}$$

The null rays in this line element follow the trajectories given by

$$0 = f\dot{t}^2 - f^{-1}\dot{r}^2 - hr^2\dot{\phi}^2, \tag{23}$$

from which the $V_{\rm eff}$ can be extracted out as

$$V_{\rm eff}(r) = \frac{f\mathbb{L}^2}{2hr^2} - \frac{\mathbb{E}^2}{2}, \tag{24}$$

or, explicitly,

$$V_{\rm eff}(r) = \frac{\mathbb{L}^2}{2r^2}\left(\frac{\beta(8q-7)Q^2 + 2qr^4}{2qr^4 + \beta Q^2}\right)\left(1 - \frac{2M}{r} - \frac{\kappa^2 r^2}{3\beta} \times \left[{}_2F_1\left(-\frac{3}{4}, -q; \frac{1}{4}; -\frac{Q^2\beta}{2qr^4}\right) - 1\right]\right) - \frac{\mathbb{E}^2}{2}, \tag{25}$$

the stationary of which corresponds to the existence of photon orbits; i.e., $V'_{\rm eff}(r) = 0$.

Since the metric function is not in a simple closed-form function, it is of little interest to determine the $r_{\rm UCO}$ and $r_{\rm SCO}$ analytically. In Figs. 5–6, we plot $V_{\rm eff}(r)$ for a photon. In the nonextremal case, the situation is similar as in RN, except in the weak-coupling regime and $q < 1$, we have $r_{\rm UCO} < r_{\rm SCO}$. Both are still inside the corresponding outer

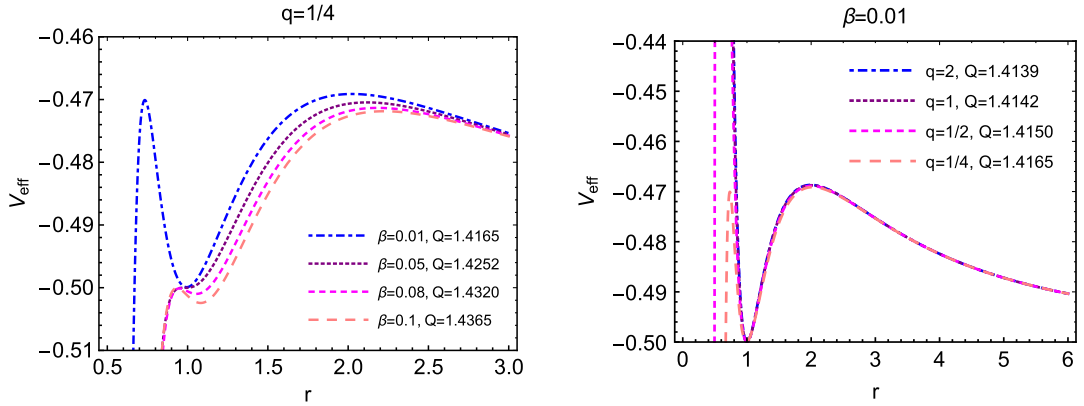

FIG. 6. The extremal case of effective potential for massless particles. [Left] $V_{\rm eff}$ with a fixed q and several values of β parameter [Right] and vice versa. We set $M = 1$.

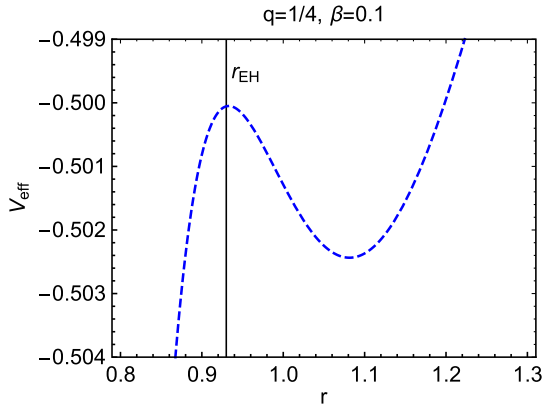

FIG. 7. The zoomed-in version of $V_{\rm eff}$ for $q = 1/4$ shown in Fig. 6. It can be observed that the inner $r_{\rm UCO}$ coincides with $r_{\rm EH}$ (as can be confirmed by Table I), while $r_{\rm SCO}$ lies outside.

horizon. For the extremal case, however, something interesting emerges. As can be seen from Fig. 6, there are typically two $r_{\rm UCO}$ and one $r_{\rm SCO}$, and the position of $r_{\rm SCO}$ shifts *farther away* from singularity when β gets stronger, as opposed to the behavior of $r_{\rm EH}$ discussed earlier. As a result, there is a window of parameter space where you can have stable photon orbits *outside* the extremal horizon; *i.e.*, $r_{\rm SCO} > r_{\rm EH}$. This is clearly shown in Fig. 7. The consequence is novel. Not only is a stable circular photon orbit possible, but there exist a family of bounded orbits with $r_{\rm min} \le r \le r_{\rm max}$, as long as $r_{\rm min} \ge r_{\rm EH}$.

As we mentioned in the previous subsection, for $q < 1$, the inner horizon ceases to exist as β gets stronger; i.e., the black hole behaves Schwarzschild-like. The relevant thing is whether $r_{\rm SCO}$ is located inside the remaining single horizon r_h. In Fig. 8, we plot the metric (left panel) as well as its corresponding $V_{\rm eff}$ for timelike (center panel) and null (right panel) in the strong-coupling limit ($\beta = 2$) and $q = 1/4$. It can be observed that the timelike $V_{\rm eff}$ possesses $r_{\rm UCO}$ and

TABLE I. Comparation of the radius of an event horizon of the extremal case ($r_{\rm EH}$) with $q = 1/4$ for various number of β, with its $r_{\rm SCO}$ and $r_{\rm SCO}$. The starred value is a saddle point.

β	Q	$r_{\rm EH}$	$r_{\rm UCO}$	$r_{\rm SCO}$
2.0	2.0	0.2900	⋯	0.4220
0.1	1.4365	0.9300	0.934 and 2.223	1.081
0.08	1.4320	0.9475	0.951 and 2.187	1.054
0.05	1.4252	0.9690	2.117	0.980*
0.01	1.4165	0.9899	0.734 and 2.023	0.994

$r_{\rm SCO}$ with $r_{\rm UCO} < r_{\rm SCO}$. On the other hand, for a null geodesic, only $r_{\rm SCO}$ exists, and $r_h < r_{\rm SCO}$. Thus, for $\beta = 2$, we infer that it is valid for a strong-coupling regime $\beta \ge 1$, and stable photon orbits also exist. In Table I, we show physical photon orbits with $r_{\rm SCO} > r_{\rm EH}$ for the case of $q = 1/4$ with varying β and the values of BH charge Q. This is a typical family of solutions with $q < 1$. For the specific $\beta = 0.05$, we found that the $r_{\rm SCO}$ is rather metastable since it is the saddle point of $V_{\rm eff}$; i.e., $V''(r_{\rm SCO}) = 0$.

C. Null geodesics in the Born-Infeld case ($q = 1/2$)

In this section, we examine the null behavior of $q = 1/2$, which reduces our model to BI electrodynamics. While the null geodesics of the BI model has been studied in the past [34,53], there are only a few extensive studies that worked on the magnetostatic scenario [54,55]. It is worth to note that the BI model enjoys $SO(2)$-duality invariance (not necessarily present in other NLED), where the spherically symmetric solution is *exactly* the same for electric and magnetic case. Breton has shown in her paper that for the electric BI model, a black hole possesses $r_{\rm SCO}$ outside the $r_{\rm EH}$ [34]. Through our study, we want to take a look if the magnetic case also performs the same result. Here, we evaluate the solution in the extremal case. The metric function $f(r)$ and its potential $V_{\rm eff}$ are shown in Figs. 9–10.

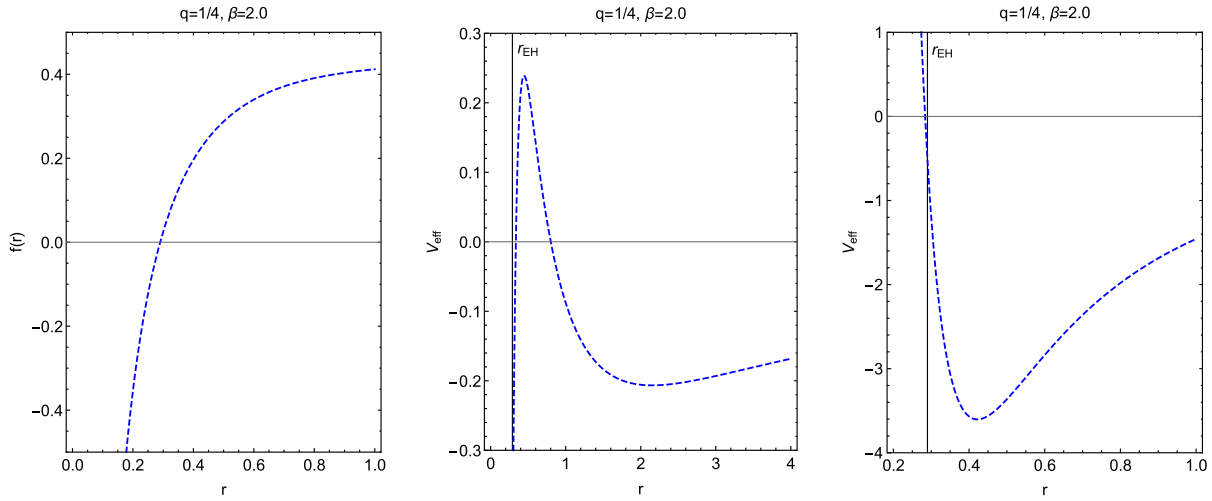

FIG. 8. The metric function $f(r)$ (left), effective potential for massive particles (center), and effective potential for light particles (right) with $M = 1$ and $Q = 2$.

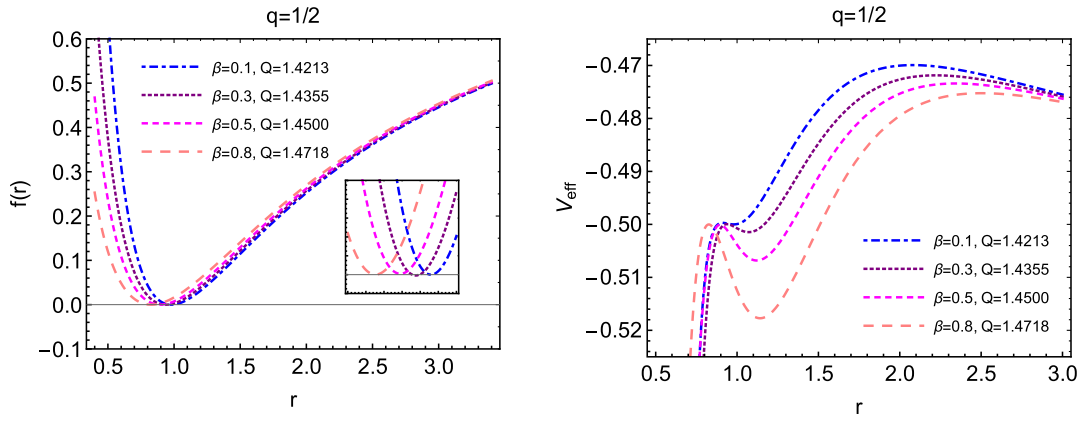

FIG. 9. [Left] The extremal case of metric function $f(r)$ and [Right] the extremal case of effective potential for massless particles with $q = 1/2$ and several values of β parameter. Here, we set $M = 1$.

Here, we see the metric behavior is similar to the previous case ($q = 1/4$). The event horizon radius $r_{\rm EH}$ gets smaller as the value of β increases. The potential, on the other hand, shows that the $r_{\rm SCO}$ moves *farther away* from the center of the black holes as β rises. We analyze the numbers, and we find that the $r_{\rm SCO}$ lies outside the event horizon for almost all values of β, where the case of $\beta = 0.1$ has the $r_{\rm EH}$, and $r_{\rm SCO}$ coincide. In Table. II, we show physical photon orbits with $r_{\rm SCO} > r_{\rm EH}$ for the case of $q = 1/2$ with varying β and the values of BH charge Q.

D. Deflection of light

As the last analysis for this model, let us calculate the (weak) deflection angle of light in the case other than the BI model. Consider the case of $q = 1/4$, knowing the conserved quantities, $\mathbb{E} = f\dot{t}$, $\mathbb{L} = hr^2\dot{\phi}$ and defining the impact parameter $b_0 = \mathbb{L}/\mathbb{E}$, we rewrite the null geodesics in terms of $u \equiv 1/r$ as

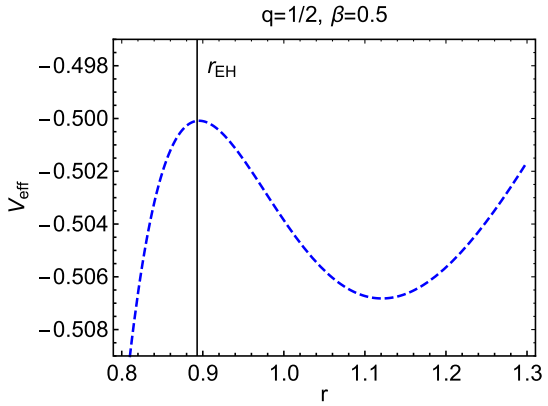

FIG. 10. The zoomed-in version of $V_{\rm eff}$ for the Born-Infeld case shown in Fig. 9. It can be observed that the inner $r_{\rm UCO}$ coincides with $r_{\rm EH}$ (as can be confirmed by Table II), while $r_{\rm SCO}$ lies outside.

$$\frac{d^2u}{d\phi^2} + fhu = -\frac{u^2}{2}\frac{d}{du}(fh) + \frac{1}{2b_0^2}\frac{d}{du}(h^2). \tag{26}$$

Assuming small $\beta \ll 1$, we might expand the metric function f and conformal factor h using the Taylor series for the first order of β. Inserting the corresponding function, Eq. (26) up to the first order in β is

$$\frac{d^2u}{d\phi^2} + u = 3Mu - \kappa^2Q^2u^3 + \beta\left(\frac{48Q^2u^3}{b_0^2} + 84MQ^2u^6 - \frac{1}{10}237\kappa^2Q^4u^7 - 36Q^2u^5\right). \tag{27}$$

Define $\epsilon \equiv Mu_0$ and $\xi \equiv u/u_0$. This yields Eq. (27), up to the second-order in ϵ,

$$\frac{d^2\xi}{d\phi^2} + \xi \approx 3\xi^2\epsilon + \xi^3\epsilon^2\left(\frac{48\beta Q^2}{\mathrm{b0}^2M^2} - \frac{\kappa^2Q^2}{M^2}\right). \tag{28}$$

Now, expand ξ in power of ϵ, $\xi = \xi_0 + \epsilon\xi_1 + \epsilon^2\xi_2 + \ldots.$, then insert them into Eq. (28). We can sort the equation by collecting terms in a different order of ϵ [38],

$$\begin{aligned}\frac{d^2\xi_0}{d\phi^2} + \xi_0 &= 0,\\ \frac{d^2\xi_1}{d\phi^2} - 3\xi_0^2 + \xi_1 &= 0,\\ \frac{d^2\xi_2}{d\phi^2} + \frac{\kappa^2\xi_0^3Q^2}{M^2} - \frac{48\beta\xi_0^3Q^2}{b_0^2M^2} - 6\xi_1\xi_0 + \xi_2 &= 0.\end{aligned} \tag{29}$$

TABLE II. Comparation of the radius of event horizon of the extremal case ($r_{\rm EH}$) in Born-Infeld case for various number of β, with its $r_{\rm SCO}$.

β	Q	$r_{\rm EH}$	$r_{\rm UCO}$	$r_{\rm SCO}$
0.1	1.4213	0.970	0.910 and 2.077	0.981
0.3	1.4355	0.935	0.937 and 2.221	1.072
0.5	1.4500	0.893	0.895 and 2.344	1.122
0.8	1.4718	0.830	0.827 and 2.502	1.142

Solving them, we find the approximation of inverse radial distance u as

$$u \simeq u_0\cos(\phi) + \frac{1}{2}Mu_0^2(3-\cos(2\phi)) + \frac{u_0^3}{32b_0^2}[12\phi\sin(\phi)(b0^2(10M^2-\kappa^2Q^2)+48\beta Q^2) + \cos(\phi)(b0^2(54M^2-7\kappa^2Q^2)+336\beta Q^2) + \cos(3\phi)(b0^2(6M^2+\kappa^2Q^2)-48\beta Q^2)]. \quad (30)$$

Asymptotically, $\phi \to \pi/2+\delta$ as $u \to 0$. For the case of $u_0 \approx 0$, we can solve δ, keeping only the second order of u_0 as

$$\delta \approx 2Mu_0 + u_0^2\left(\frac{9\pi\beta Q^2}{b_0^2}+\frac{15\pi M^2}{8}-\frac{3}{16}\pi\kappa^2Q^2\right). \quad (31)$$

We want to see the contribution of the first order β in the deflection angle. We use $b_0 \approx 1/u_0 \equiv r_{tp}$, where r_{tp} is the radius of the turning point. The weak deflection angle can be obtained as

$$\Delta\phi_{\text{weak}} \equiv 2\delta \approx \frac{4M}{r_{\text{tp}}}+\frac{15\pi M^2}{4r_{\text{tp}}^2}+Q^2\left(\frac{18\pi\beta}{r_{\text{tp}^4}}-\frac{3\pi\kappa^2}{8r_{\text{tp}}^2}\right). \quad (32)$$

Using the same method, the deflection angle for other cases of q is calculated. The behavior is shown in Fig. 11.

In Fig. 11 above, we show the behavior of deflection angles by setting the value of its parameter with $M = 10\ M_\odot$ (solar mass), setting the charge (arbitrarily) to be $Q = 0.3$, and the radius of the turning point $r_{tp} = b$ in asolar radius $r_\odot$, which has been normalized by a Schwarzchild radius r_S. It can be seen that the other cases beside the Maxwell ($q \neq 1$) lay on the same curves. They all asymptote to Maxwell for large r_{tp}, as they should, but significantly differ in the short-length regime. The extra term of β contributes a bigger value of the deflection angle near the Schwarzchild radius. Obviously, we cannot trust this weak approximation all the way to $r_{tp} = r_S$, since it is the regime where the field gets strong, and thus, full strong deflection analysis is required [56–59].

IV. POWER-LAW NLED

This power-law electrodynamics was proposed by Hassaine and Martinez [30,31] and is given by

$$\mathcal{L} = -\mathcal{F}^q. \quad (33)$$

Maxwell is recovered when $q = 1$. The corresponding "permittivity" and "permeability" are expressed as

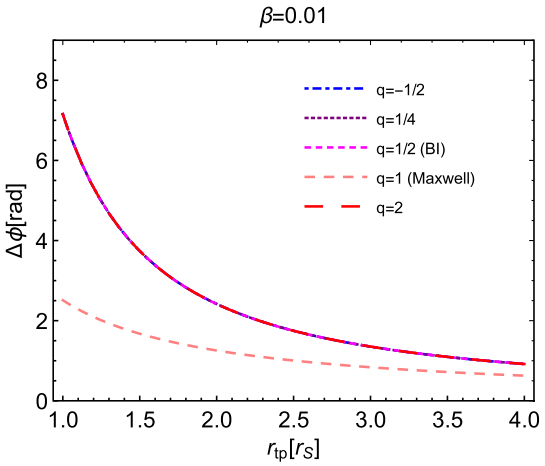

FIG. 11. Deflection angles for various number of q.

$$\epsilon_m = \mu_m^{-1} = q\mathcal{F}^{q-1}. \quad (34)$$

They found that the BH is given by

$$f(r) = 1-\frac{2M}{r}-\frac{\kappa^2 2^{-q}r^2}{3-4q}\left(\frac{Q^2}{r^4}\right)^q. \quad (35)$$

It can be seen at a glance that $q \neq 3/4$. The typical plots of $f(r)$ is shown in Fig. 12. Asymptotically, $f(r)$ goes as

$$\lim_{r\to\infty} f(r) = \begin{cases} 1, & q > 1/2, \\ 1-\frac{1}{\sqrt{2}}, & q = 1/2, \\ -\infty, & q < 1/2. \end{cases}$$

Thus, the black hole is asymptotically flat only for $q > 1/2$. The case of $q = 1/2$ is unique as it goes to flat but differs from Minkowski at a large distance [30,31].

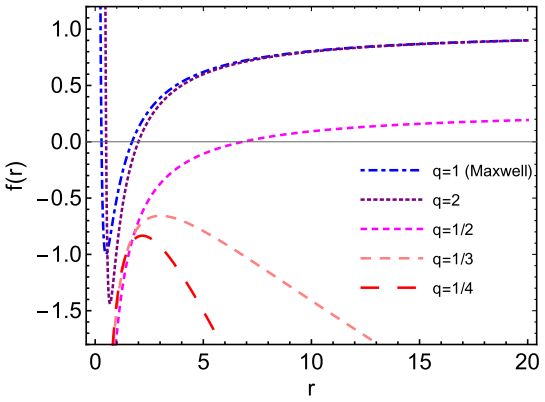

FIG. 12. Metric function $f(r)$ with $Q = M = 1$.

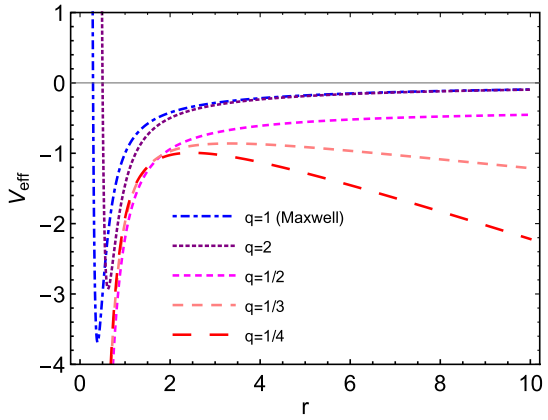

FIG. 13. The effective potential for massive particles with $M = 1$, $Q = 1$, and $\mathbb{E} = \mathbb{L} = 1$.

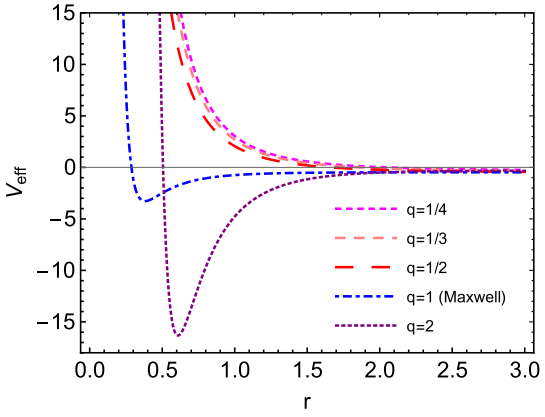

FIG. 14. The effective potential for light particles with $M = 1$, $Q = 1$, and $\mathbb{E} = \mathbb{L} = 1$.

A. Timelike geodesics

The corresponding $V_{\rm eff}$ for massive test particles is

$$V_{\rm eff}(r) = \frac{1}{2}\left(\frac{\mathbb{L}^2}{r^2}+1\right)\left[1-\frac{2M}{r}-\frac{\kappa^2 2^{-q} r^2}{3-4q}\left(\frac{Q^2}{r^4}\right)^q\right]-\frac{\mathbb{E}^2}{2}. \tag{36}$$

Asymptotically,

$$\lim_{r\to\infty} V_{\rm eff}(r) = \begin{Bmatrix} 0, & q > 1/2, \\ -\frac{1}{2\sqrt{2}}, & q = 1/2, \\ -\infty, & q < 1/2. \end{Bmatrix}.$$

The $V_{\rm eff}$ behaves quite similarly with the metric, as shown in Fig. 13. No stable or unstable orbit exists outside the horizon.

B. Null geodesics

The effective geometry in this model is given by

$$g^{\mu\nu}_{\rm eff} = g^{\mu\nu} - \frac{4}{(q-1)\mathcal{F}} F^{\mu\alpha}F^{\nu}_{\alpha}. \tag{37}$$

The line element can be written as Eq. (21) but with $h(r) \equiv (8q-7)^{-1}$. The corresponding effective potential is

$$V_{\rm eff}(r) = \frac{(8q-7)\mathbb{L}^2}{2r^2}\left(1-\frac{2M}{r}-\frac{\kappa^2 2^{-q} r^2}{3-4q}\left(\frac{Q^2}{r^4}\right)^q\right)-\frac{\mathbb{E}^2}{2}. \tag{38}$$

In Fig. 14, we show the uninteresting result of $V_{\rm eff}$, since no photon orbit (stable or unstable) exists either. In the following discussion, we shall show that this power-law NLED model is problematic phenomenologically, at least in the weak-deflection limit.

C. Deflection of light

For this model, it is easier to calculate the deflection angle through the first-order, rather than the second-order as done previously, differential equation. Recalling the null geodesics equation (23) and substituting $u = 1/r$, the term $\dot{r}$ can be rewritten as

$$\dot{r}^2 = \left(\frac{dr}{d\phi}\frac{d\phi}{d\tau}\right) = \mathbb{L}^2\left(\frac{du}{d\phi}\right)^2. \tag{39}$$

Equation (23) then becomes

$$\left(\frac{du}{d\phi}\right)^2 = \frac{1}{b^2}-\frac{fu^2}{h}. \tag{40}$$

Defining $\sigma(u) \equiv bu(f/h)^{1/2}$, we obtain

$$\frac{du}{d\phi} = \frac{1}{b}(1-\sigma^2)^{1/2}. \tag{41}$$

As an example, let us take $q = 2$. In the weak-field limit, we obtain

$$bdu = \left(\frac{1}{3}+\frac{2M\sigma}{9b}-\frac{7\kappa^2 Q^4\sigma^6}{87480b^6}\right)d\sigma. \tag{42}$$

The total change of angle ϕ with respect to u from infinity ($u = 0$) to the minimum radius ($u = u_0 = 1/b$) and back to infinity can be written as

$$\begin{aligned}\delta\phi &= 2\int_0^{u_0}\frac{d\phi}{du}du = 2\int_0^{u_0} b(1-\sigma^2)^{-1/2}du \\ &= 2\int_0^1 (1-\sigma^2)^{-1/2}\left(\frac{1}{3}+\frac{2M\sigma}{9b}-\frac{7\kappa^2 Q^4\sigma^6}{87480b^6}\right)d\sigma.\end{aligned} \tag{43}$$

The total deflection angle is defined as $\Delta\phi \equiv \delta\phi - \pi$. Using this method, we calculate the angles for several q as follows:

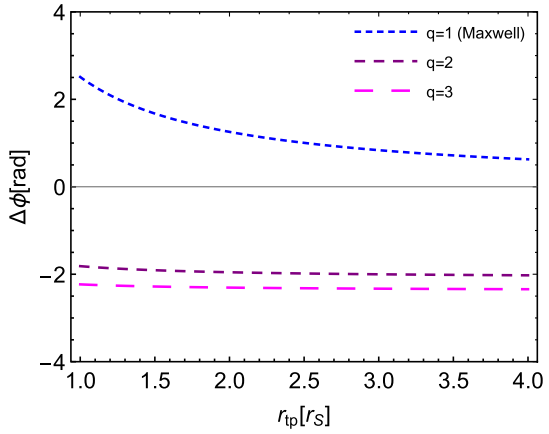

FIG. 15. Deflection angles for various number of q. Here, we set $M = 10\ M_\odot$ and $Q = 0.3$.

$$\Delta\phi(q=1) = \frac{4M}{b} + \frac{3\pi\kappa Q^2}{8b^2},$$
$$\Delta\phi(q=2) = \frac{4M}{9b} + \pi\left(-\frac{7\kappa^2 Q^4}{279936b^6} - \frac{2}{3}\right),$$
$$\Delta\phi(q=3) = \frac{4M}{17b} + \pi\left(-\frac{77\kappa^2 Q^6}{5815734272\sqrt{17}b} + \frac{1}{\sqrt{17}} - 1\right). \tag{44}$$

As can be seen from the result above, unless $q = 1$, the deflection angle does not reduce to Schwarszchild even in the limit of $Q \to 0$. What is more problematic is that as shown in Fig. 15, the angles are generically negative and do not go to zero at large r_{tp}! This correspondence violation poses a doubt whether this result is physical or not. At best, we can say that the weak-field approximation seems to break down for this model.

V. AYON-BEATO-GARCIA BLACK HOLE

In 1968, Bardeen [60] in his seminal proceeding paper published his famous *regular black hole* solution,

$$f(r) = 1 - \frac{2Mr^2}{(r^2+Q^2)^{3/2}}. \tag{45}$$

The metric is regular at the origin, as in Fig. 16. The black hole regularity is ensured by the fact that the corresponding invariants are also regular everywhere. Ayon-Beato and Garcia [44] were the first to realize that such a solution can be interpreted as a black hole charged with a NLED magnetic monopole, whose Lagrangian is given by

$$\mathcal{L} = -\frac{3}{s\kappa^2 Q^2}\left(\frac{\sqrt{2Q^2\mathcal{F}}}{1+\sqrt{2Q^2\mathcal{F}}}\right)^{5/2}, \tag{46}$$

$s \equiv Q/2M$. Its electrically charged counterpart solution was later proposed by Rodrigues and Silva [46]. Being an NLED BH, we shall study the null geodesic structure of Ayon-Beato-Garcia (ABG) metric and investigate the stable photon orbits.

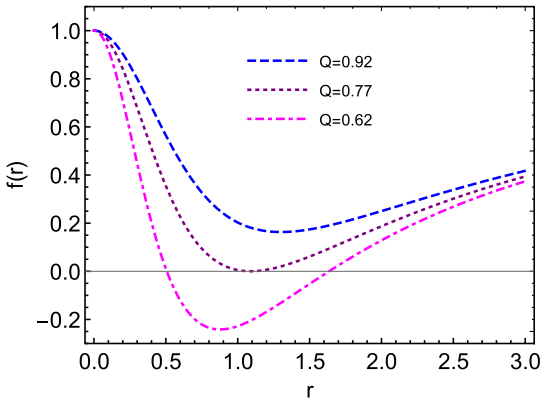

FIG. 16. Metric function for ABG black hole solution (45) with $M = 1$ and several values of Q.

A. Timelike and null geodesics

The explicit form of the ABG's timelike geodesics can be written as

$$V_{\rm eff}(r) = \frac{1}{2}\left(\frac{\mathbb{L}^2}{r^2}+1\right)\left(1-\frac{2Mr^2}{(r^2+Q^2)^{3/2}}\right) - \frac{\mathbb{E}^2}{2}. \tag{47}$$

This $V_{\rm eff}$ allows (marginally) stable orbits for massive test particles, as can be seen in the right panel of Fig. 17.

While the null geodesics structure of the original Bardeen spacetime was investigated by numerous authors (see, for example, [58,61–64]), none assumes the NLED perspective. They thus neglected the photon's effective geometry and considered a photon and graviton to follow the same null rays. Consequently, no stable photon sphere is observed by an observer outside the horizon. Here, we follow the ABG's perspective and found something novel.

From the Lagrangian [Eq. (46)], the effective metric can be written as

$$g^{\mu\nu}_{\rm eff} = g^{\mu\nu} + \frac{2r^4(6Q^4+5Q^2r^2-1)}{Q^2(Q^2+r^2)^2}F^{\mu\alpha}F^{\nu}_{\alpha}. \tag{48}$$

Defining $h(r) \equiv (1 - \frac{2(6Q^4+5Q^2r^2-1)}{(Q^2+r^2)^2})^{-1}$, the effective potential can be obtained,

$$V_{\rm eff}(r) = \frac{\mathbb{L}^2}{2r^2}\left(1-\frac{2(6Q^4+5Q^2r^2-1)}{(Q^2+r^2)^2}\right) \times \left(1-\frac{2Mr^2}{(r^2+Q^2)^{3/2}}\right) - \frac{\mathbb{E}^2}{2}. \tag{49}$$

The circular orbit radii satisfy

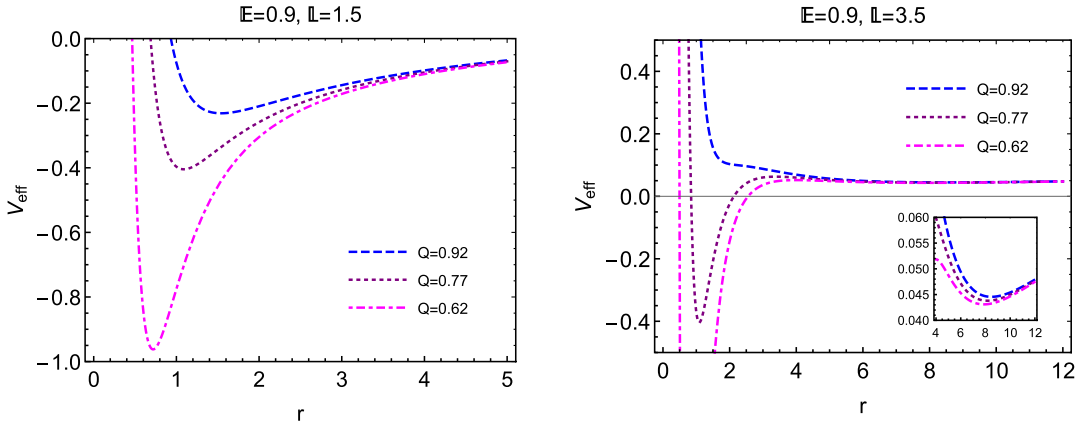

FIG. 17. The effective potential for massive particles with $M = 1$ for a various number of Q.

$$0 = \frac{\mathbb{L}\left(\frac{4r(12Q^4+10Q^2r^2-2)}{(Q^2+r^2)^3} - \frac{20Q^2r}{(Q^2+r^2)^2}\right)\left(1 - \frac{2Mr^2}{(Q^2+r^2)^{3/2}}\right)}{2r^2} + \frac{\mathbb{L}\left(1 - \frac{12Q^4+10Q^2r^2-2}{(Q^2+r^2)^2}\right)\left(\frac{6Mr^3}{(Q^2+r^2)^{5/2}} - \frac{4Mr}{(Q^2+r^2)^{3/2}}\right)}{2r^2} - \frac{\mathbb{L}\left(1 - \frac{12Q^4+10Q^2r^2-2}{(Q^2+r^2)^2}\right)\left(1 - \frac{2Mr^2}{(Q^2+r^2)^{3/2}}\right)}{r^3}. \tag{50}$$

Finding its analytical roots is not illuminating. We thus determine the $r_{\rm SCO}$ by studying Fig. 18. It can be seen that for the case of extremal and two horizons, there are minima, albeit of little depth, whose $r_{\rm SCO} > r_h$. This means that an ABG BH allows stable photon orbits. The detail numerical values of the corresponding radii are shown in Table. III. This stability is considered to be marginally stable, since the depth of minima is quite shallow. Nevertheless, it is not a problem classically.

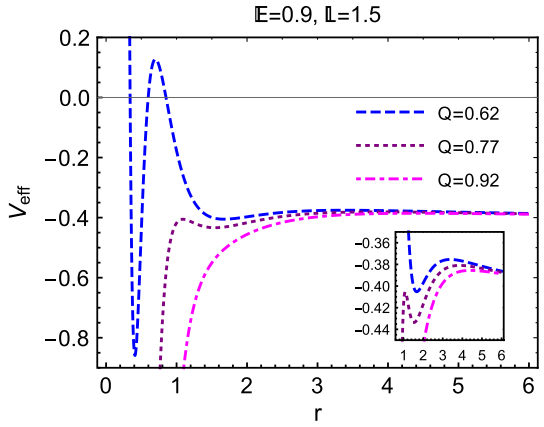

FIG. 18. The effective potential for light particles with $M = 1$ for a various number of Q. The corresponding equation is Eq. (49).

B. Deflection of light

Finally, let us calculate the deflection angle of a photon off the ABG black hole which, to the best of our knowledge, has not been studied in the literature. In the limit of small Q, the inverse radial distance is, approximately,

$$u \simeq \frac{u_0^3}{32\alpha^2}(12\sqrt{\alpha}\phi\sin(\sqrt{\alpha}\phi)((\alpha-1)\alpha b_0^2 + 10M^2) + \cos(\sqrt{\alpha}\phi)(7(\alpha-1)\alpha b_0^2 + 54M^2) + \cos(3\sqrt{\alpha}\phi)(6M^2 - (\alpha-1)\alpha b_0^2)) + \frac{Mu_0^2}{4\alpha}(9\sin^2(\sqrt{\alpha}\phi) + \sin(\sqrt{\alpha}\phi)\sin(3\sqrt{\alpha}\phi) + 4\cos^4(\sqrt{\alpha}\phi)) + u_0\cos(\sqrt{\alpha}\phi), \tag{51}$$

where we define $\alpha \equiv 1 - \frac{20Q^2}{b_0^2}$. For $\alpha \approx 1$, the weak deflection angle is given by

$$\Delta\phi_{\rm weak} \approx \frac{8M}{r_{tp}} + \frac{15\pi M^2}{2r_{tp}^2} + \mathcal{O}(Q^2). \tag{52}$$

The zeroth order is twice the Schwarzschild's angle. This is because ABG describes a regular (Bardeen) black hole, which is distinct from Schwarzschild. The dependence of $\Delta\phi$ on r_{tp} is shown in Fig. 19. This might be used to distinguish the ABG/Bardeen's signature from another ordinary black hole.

TABLE III. Comparation of the radius of event horizon of the extremal case ($r_{\rm EH}$) Q, next to its corresponding values of $r_{\rm SCO}$ and $r_{\rm SCO}$ of the null geodesics.

Q	r_h	$r_{\rm UCO}$	$r_{\rm SCO}$
0.62	0.5065 and 1.6349	0.6994 and 3.3887	0.4097 and 1.6743
0.77	1.0887	1.0897 and 3.8556	1.54353
0.92	⋯	4.4158	⋯

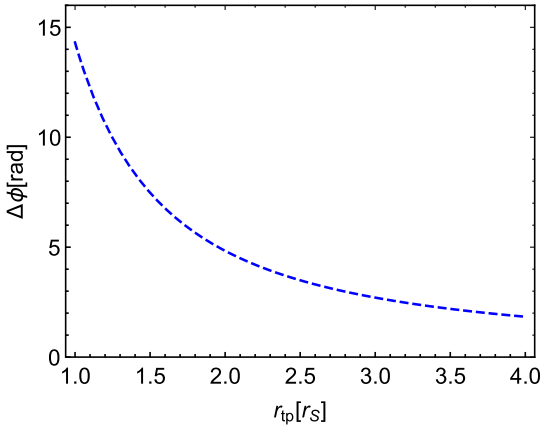

FIG. 19. Deflection angles of ABG black holes.

VI. CONCLUSION

This work is intended to investigate the null geodesic of several NLED black holes and its phenomenological aspects. In this work, we specifically consider three polynomial-type NLED models: the generalized BI model (we dubbed it the Kruglov-BI model), the power-law model, and the Ayon-Beato-Garcia model used in a Bardeen black hole. Each has been extensively studied by a large number of authors. What is left uninvestigated, and this is our main result, is the behavior of a photon around them. Due to the field discontinuity, a photon follows the null geodesic that is different from a graviton in NLED theories. Our simple investigation shows novel results.

In the first model, we show that in the extremal limit of some weak coupling β, the black hole allows stable physical photon orbits. By *physical*, we mean that the orbits lie outside the horizon. For the strong coupling $\beta < 1$, generically for $q < 1$, the black hole only possesses one horizon, and we show that there is a range of parameters that also allows this case to have stable physical orbits for a photon. The results are genuine, since an extremal RN black hole has a stable photon orbit with a $r_{\rm SCO}$ that coincides with $r_{\rm EH}$. It is not clear how stable this is since any small perturbation might collapse the photon inside the horizon. Now, the possibility of having $r_{\rm SCO} > r_{\rm EH}$ in the NLED case evades such concern. Not only do we now have stable circular orbits, but also there exist a family of bounded orbits parametrized by two radii, r_+ and r_-, as long as $r_- \geq r_{\rm EH}$. In Newtonian gravity, these closed orbits would correspond to ellipses. In GR, however, to determine the orbits, we must explicitly solve the null geodesic equation. This is left for our future investigation.

For the second model, we found problematic phenomenological results since the weak deflection angle does not coincide with Schwarzschild even in the chargeless limit ($Q \to 0$). We argue that such a model is unphysical, even though we do not eliminate the possibility that our weak-gravitational field approach might be a breakdown for this model. At best, we can say that the weak-field analysis fails, and one must resort to the full strong deflection analysis to get a satisfactory answer.

The last model deals with the ABG metric that gives rise to a regular black hole. A regular black hole was first proposed, to our best knowledge, by Bardeen. Later, Ayon-Beato and Garcia realized that such a solution can be perceived as a black hole endowed with a NLED magnetic charge. An interesting aspect is that, while the metric solution and the timelike geodesic between Bardeen and ABBG are equivalent, the null geodesic is not. Perceived as an original Bardeen, a regular BH has the usual property that a photon follows its null geodesic. The study of its null geodesic showed that the corresponding $V_{\rm eff}$ possesses singularity [65]; therefore, it is futile to talk about a photon orbit around a Bardeen BH. But looking from the NLED perspective, the matter becomes nontrivial. A test photon follows its effective geometry, and our investigation reveals that it is nonsingular. Similar to the Kruglov-BI case, the ABG black hole also allows a photon sphere and other bounded orbits outside the horizon. Our calculation on the weak deflection angle shows that up to zeroth order, it is twice the Schwarzschild value. While we argue that this might be caused by the fact that the two have different natures regarding the singularity (thus, the effective null geodesic outside the horizon is influenced by the nature inside it), we also realize that the strong deflection formalism is needed to have a conclusive hypothesis.

ACKNOWLEDGMENTS

We thank Byon Jayawiguna, Reyhan Lambaga, Ilham Prasetyo, and Haryanto Siahaan for fruitful discussions. We are also grateful for the referee's comments and suggestions to the first manuscript. This work is partially funded by Hibah PUTI Q1 UI 2020 Grant No. NKB-1373/UN2.RST/HKP.05.00/2020.

[1] K. Akiyama *et al.* (Event Horizon Telescope Collaboration), First M87 Event Horizon Telescope Results. I. The Shadow of the Supermassive Black Hole, Astrophys. J. **875**, L1 (2019); **875**, L2 (2019); **875**, L3 (2019); **875**, L4 (2019); **875**, L5 (2019).

[2] E. Teo, Spherical photon orbits around a Kerr black hole, Gen. Relativ. Gravit. **35**, 1909–1926 (2003).

[3] M. Bugden, Spherical photon orbits around a 5D MyersPerry black hole, Gen. Relativ. Gravit. **50**, 30 (2018).

[4] P. Pradhan and P. Majumdar, Circular Orbits in Extremal Reissner Nordstrom Spacetimes, Phys. Lett. A **375**, 474 (2011).

[5] F. S. Khoo and Y. C. Ong, Lux in obscuro: Photon Orbits of Extremal Black Holes Revisited, Classical Quantum Gravity **33**, 235002 (2016) [Erratum, Classical Quantum Gravity**34**, 219501 (2017)].

[6] A. A. Chernitskii, Born-Infeld equations, arXiv: hep-th/0509087.

[7] M. Born and L. Infeld, Foundations of the new field theory, Proc. R. Soc. A **144**, 425 (1934).

[8] C. Bamber *et al.*, Studies of nonlinear QED in collisions of 46.6-GeV electrons with intense laser pulses, Phys. Rev. D **60**, 092004 (1999).

[9] D. Tommasini, A. Ferrando, H. Michinel, and M. Seco, Detecting photon-photon scattering in vacuum at exawatt lasers, Phys. Rev. A **77**, 042101 (2008).

[10] O. J. Pike, F. Mackenroth, E. G. Hill, and S. J. Rose, A photonphoton collider in a vacuum hohlraum, Nat. Photonics **8**, 434 (2014).

[11] P. Gaete and J. Helayël-Neto, Remarks on nonlinear Electrodynamics, Eur. Phys. J. C **74**, 3182 (2014).

[12] W. Heisenberg and H. Euler, Consequences of Dirac's theory of positrons, Z. Phys. **98**, 714 (1936).

[13] R. Battesti and C. Rizzo, Magnetic and electric properties of quantum vacuum, Rept. Prog. Phys. **76**, 016401 (2013).

[14] A. Cadène, P. Berceau, M. Fouché, R. Battesti, and C. Rizzo, Vacuum magnetic linear birefringence using pulsed fields: status of the BMV experiment, Eur. Phys. J. D **68**, 16 (2014).

[15] F. D. Valle, E. Milotti, A. Ejlli, G. Messineo, L. Piemontese, G. Zavattini, U. Gastaldi, R. Pengo, and G. Ruoso, First results from the new PVLAS apparatus: A new limit on vacuum magnetic birefringence, Phys. Rev. D **90**, 092003 (2014).

[16] S. I. Kruglov, On generalized Born-Infeld electrodynamics, J. Phys. A **43**, 375402 (2010).

[17] S. I. Kruglov, Notes on BornInfeld-type electrodynamics, Mod. Phys. Lett. A **32**, 1750201 (2017).

[18] S. Kruglov, Commun. Theor. Phys. **66**, 59–65 (2016) doi: https://doi.org/10.1088/0253-6102/66/1/059.

[19] S. I. Kruglov, Universe **5**, 225 (2019).

[20] J. Y. Kim and T. Lee, J. Cosmol. Astropart. Phys. 11 (2011) 017 doi: https://doi.org/10.1088/1475-7516/2011/11/017.

[21] S. Kruglov, Mod. Phys. Lett. A **32**, 1750092 (2017) doi: https://doi.org/10.1142/S0217732317500924.

[22] P. Gaete and J. Helayël-Neto, Finite Field-Energy and Interparticle Potential in Logarithmic Electrodynamics, Eur. Phys. J. C **74**, 2816 (2014).

[23] S. I. Kruglov, On Generalized Logarithmic Electrodynamics, Eur. Phys. J. C **75**, 88 (2015).

[24] A. Sheykhi and Z. Abdollahzadeh, Effects of Exponential Nonlinear Electrodynamics and External Magnetic Field on Holographic Superconductors, Int. J. Theor. Phys. **57**, 917 (2018).

[25] S. I. Kruglov, Black hole as a magnetic monopole within exponential nonlinear electrodynamics, Ann. Phys. **378**, 59 (2017).

[26] A. Sheykhi and F. Shaker, Effects of backreaction and exponential nonlinear electrodynamics on the holographic superconductors, Int. J. Mod. Phys. D **26**, 1750050 (2017).

[27] B. Hoffmann and L. Infeld, On the choice of the action function in the new field theory, Phys. Rev. **51**, 765 (1937).

[28] A. Peres, Nonlinear Electrodynamics in General Relativity, Phys. Rev. **122**, 273 (1961).

[29] S. Fernando and D. Krug, Charged black hole solutions in Einstein-Born-Infeld gravity with a cosmological constant, Gen. Relativ. Gravit. **35**, 129 (2003).

[30] M. Hassaine and C. Martinez, Higher-dimensional charged black holes solutions with a nonlinear electrodynamics source, Classical Quantum Gravity **25**, 195023 (2008).

[31] M. Hassaine and C. Martinez, Higher-dimensional black holes with a conformally invariant Maxwell source, Phys. Rev. D **75**, 027502 (2007).

[32] K. A. Bronnikov, Regular magnetic black holes and monopoles from nonlinear electrodynamics, Phys. Rev. D **63**, 044005 (2001).

[33] S. I. Kruglov, Nonlinear Electrodynamics and Magnetic Black Holes, Ann. Phys. **529**, 1700073 (2017).

[34] N. Breton, Born-Infeld generalization of the Reissner-Nordstrom black hole, arXiv: gr-qc/0109022.

[35] S. I. Kruglov, BornInfeld-type electrodynamics and magnetic black holes, Annals Phys. **383**, 550 (2017).

[36] S. H. Hendi, S. Panahiyan, and E. Mahmoudi, Thermodynamic analysis of topological black holes in Gauss-Bonnet gravity with nonlinear source, Eur. Phys. J. C **74**, 3079 (2014).

[37] S. H. Hendi, S. Panahiyan, and B. Eslam Panah, PV criticality and geometrical thermodynamics of black holes with BornInfeld type nonlinear electrodynamics, Int. J. Mod. Phys. D **25**, 1650010 (2016).

[38] S. Jana and S. Kar, Born-Infeld gravity coupled to Born-Infeld electrodynamics, Phys. Rev. D **92**, 084004 (2015).

[39] S. I. Kruglov, Phys. Rev. D **92**, 123523 (2015) doi: https://doi.org/10.1103/PhysRevD.92.123523.

[40] G. C. Samanta, S. K. Biswal, and K. Bamba, arXiv:1810.01874.

[41] S. Hendi, Prog. Theor. Phys. **124**, 493–502 (2010) doi: https://doi.org/10.1143/PTP.124.493.

[42] A. Sheykhi, Phys. Rev. D **86**, 024013 (2012) doi: https://doi.org/10.1103/PhysRevD.86.024013.

[43] E. Ayon-Beato and A. Garcia, Phys. Rev. Lett. **80**, 5056–5059 (1998) doi: https://doi.org/10.1103/PhysRevLett.80.5056.

[44] E. Ayon-Beato and A. Garcia, Phys. Lett. B **493**, 149–152 (2000) doi: https://doi.org/10.1016/S0370-2693(00)01125-4.

[45] H. Ghaffarnejad, M. Amirmojahedi, and H. Niad, Adv. High Energy Phys. **2018**, 1 (2018) doi: https://doi.org/10.1155/2018/3067272.

[46] M. E. Rodrigues and M. V. d. Silva, J. Cosmol. Astropart. Phys. 06 (2018), 025 doi: https://doi.org/10.1088/1475-7516/2018/06/025.

[47] M. Novello, V. A. De Lorenci, J. M. Salim, and R. Klippert, Geometrical aspects of light propagation in nonlinear electrodynamics, Phys. Rev. D **61**, 045001 (2000).

[48] Y. M. Xu, H. M. Wang, Y. X. Liu, and S. W. Wei, Photon sphere and reentrant phase transition of charged Born-Infeld-AdS black holes, Phys. Rev. D **100**, 104044 (2019).
[49] H. Li, Y. Chen, and S. J. Zhang, Photon orbits and phase transitions in Born-Infeld-dilaton black holes, arXiv: 1908.09570.
[50] A. E. Shabad and V. V. Usov, Effective Lagrangian in nonlinear electrodynamics and its properties of causality and unitarity, Phys. Rev. D **83**, 105006 (2011).
[51] S. I. Kruglov, Magnetized black holes and nonlinear electrodynamics, Int. J. Mod. Phys. A **32**, 1750147 (2017).
[52] I. H. Salazar, A. Garcia, and J. Plebanski, Duality Rotations and Type *D* Solutions to Einstein Equations With Nonlinear Electromagnetic Sources, J. Math. Phys. **28**, 2171 (1987).
[53] S. Fernando, Remarks on null geodesics of Born-Infeld black holes, ISRN Math. Phys. **2012**, 869069 (2012).
[54] N. Breton, Stability of nonlinear magnetic black holes, Phys. Rev. D **72**, 044015 (2005).
[55] N. Breton and R. Garcia-Salcedo, Nonlinear Electrodynamics and black holes, arXiv:hep-th/0702008.
[56] V. Bozza, S. Capozziello, G. Iovane, and G. Scarpetta, Strong field limit of black hole gravitational lensing, Gen. Relativ. Gravit. **33**, 1535 (2001).
[57] V. Bozza, Gravitational lensing in the strong field limit, Phys. Rev. D **66**, 103001 (2002).
[58] E. F. Eiroa and C. M. Sendra, Gravitational lensing by a regular black hole, Classical Quantum Gravity **28**, 085008 (2011).
[59] E. F. Eiroa, Gravitational lensing by Einstein-Born-Infeld black holes, Phys. Rev. D **73**, 043002 (2006).
[60] J. M. Bardeen, in *Conference Proceedings of GR5* (Tbilisi, USSR, 1968), p. 174.
[61] H. Ghaffarnejad and H. Niad, Weak Gravitational lensing from regular Bardeen black holes, Int. J. Theor. Phys. **55**, 1492 (2016).
[62] S. Zhou, J. Chen, and Y. Wang, Geodesic Structure of Test Particle in Bardeen Spacetime, Int. J. Mod. Phys. D **21**, 1250077 (2012).
[63] Z. Stuchlík and J. Schee, Circular geodesic of Bardeen and AyonBeatoGarcia regular black-hole and no-horizon spacetimes, Int. J. Mod. Phys. D **24**, 1550020 (2015).
[64] J. Schee and Z. Stuchlik, Gravitational lensing and ghost images in the regular Bardeen no-horizon spacetimes, J. Cosmol. Astropart. Phys. 06 (2015) 048.
[65] M. Novello, S. E. Perez Bergliaffa, and J. M. Salim, Singularities in general relativity coupled to nonlinear electrodynamics, Classical Quantum Gravity **17**, 3821 (2000).